GYRO-SYNCHROTRON EMISSION IN A MAGNETIC DIPOLE FIELD FOR THE APPLICATION TO THE CENTER-TO-LIMB VARIATION OF MICROWAVE IMPULSIVE BURSTS

TATSUO TAKAKURA and EUGENIO SCALISE, JR.*
Tokyo Astronomical Observatory, University of Tokyo, Mitaka, Tokyo, Japan

(Received 5 September, 1969)

Abstract. In order to interpret the observed center to limb variations of spectrum and polarization of microwave impulsive bursts, gyro-synchrotron emission from nonthermal electrons trapped in a magnetic dipole field is computed. The theoretical spectrum and polarization are consistent with observed ones if we put an outer boundary of the radio source at a layer of 100–60 G or (7–9) $\times 10^4$ km in height. Rather small observed center-limb variations in intensity and polarization are attributed to the distribution of θ, an angle between the magnetic field and the direction of observer, in the radio source emitting the burst, though the intensity and polarization depend strongly on θ especially at small values of θ.

1. Introduction

The statistical analyses of center to limb variation of the characteristics of microwave impulsive bursts have been made by Kakinuma *et al.* (1969) and also by Scalise (1970). It is shown that the statistical center-limb variation in intensity is not great, although their results are not in agreement quantitatively. Kakinuma *et al.* obtained a statistical intensity ratio between the bursts near the limb and near the disk center by a factor of 0.7–0.6 at all frequencies between 9.4 GHz and 1 GHz, while Scalise obtained the factors 1.5 at 9.4 GHz, 0.7 at 3.75 GHz, 1.0 at 2 GHz and 1.5 at 1 GHz. It is also shown statistically that the degree of circular polarization is slightly smaller for the microwave impulsive bursts occurring near the limb than the bursts near the center.

If the magnetic field is almost uniform in an effective source of the microwave impulsive burst which is attributed to gyro-synchrotron emission, we may expect great center-limb variations in intensity and polarization degree, since the emissivity and polarization depend strongly on the angle between the magnetic field and the direction of observer especially at small angles. In order to account for the observed little center-limb variation in intensity, a distribution of the magnetic field in the radio source emitting the burst should be taken into account. As the model of the magnetic field in the radio source, a dipole field is adopted in the following calculation.

2. Model of the Burst Source

The magnetic field due to a bipolar sunspot is represented, for simplicity, by two *independent* axially symmetric dipole fields which have opposite polarities and are

* Present address: Center of Radio Astronomy, Universidade Mackenzie, Brasil.

Solar Physics **11** (1970) 434–455.

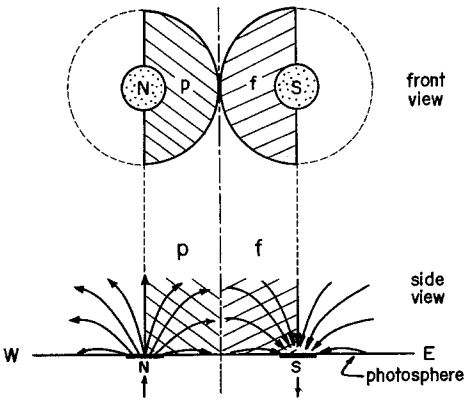

Fig. 1. Model of radio source emitting a microwave impulsive burst in a bipolar magnetic field. Two independent dipole magnetic fields with opposite senses are separated by a vertical plane shown by a chain line. Each dipole field is thus assumed to be axially symmetric about the dipole axis. Hatched regions show the radio source in which non-thermal electrons are trapped. More detail of the preceding half (p) of the radio source is shown in Fig. 2.

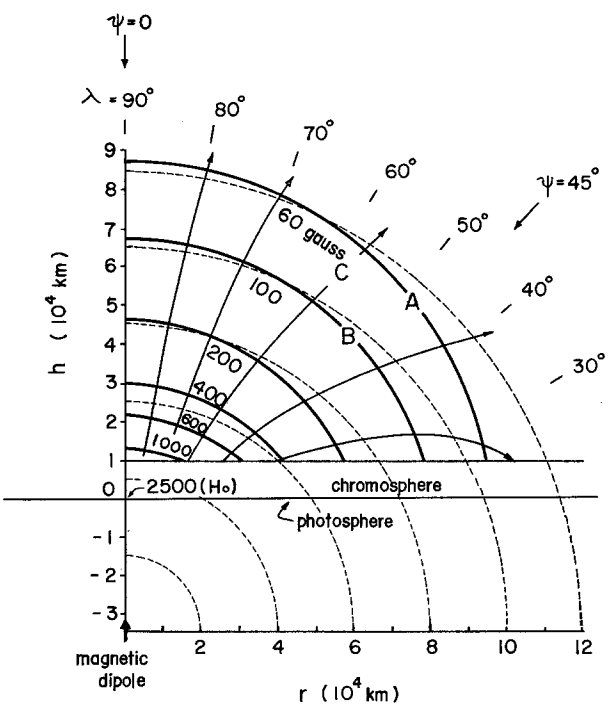

Fig. 2. Model of magnetic field in the radio source showing a cross section in the ecliptic plane. A vertical magnetic dipole is situated 3.5×10^4 km (≈ 0.05 solar radii) below the photosphere. Equi-strength surfaces of the magnetic field which are axially symmetric about the dipole axis are shown by solid curves. Curves with an arrow indicate lines of magnetic force. ψ is an angle between the axis of the dipole and the direction of observer, in other words it indicates heliographic longitude of the burst source.

bounded by a vertical plane as indicated by a chain line in Figure 1. The energetic electrons emitting a microwave impulsive burst as the gyro-synchrotron emission are assumed to be trapped in the hatched regions (p and f in Figure 1). These electrons have power law energy distribution and their number density is homogeneous in the whole radio source having an isotropic pitch angle distribution. The later condition may be satisfied by the Liouville's theory, even if the magnetic field is not uniform in the radio source like the present model (e.g., Chang and Davis, 1962).

More detail about the model of sunspot field is illustrated in Figure 2. The magnetic field is due to a vertical dipole located at 3.5×10^4 km (about 0.05 solar radii) under the photosphere and the magnetic field at the photosphere is set to 2500 G.

The chromosphere with a thickness of 10^4 km is assumed, for simplicity, to be opaque for the radio waves under consideration due to the low temperature and high density. Therefore, a lower boundary of the radio source emitting the burst is the top of the chromosphere. In the radio source, the number density of the thermal electrons N_0 is set to 10^9 cm^{-3} and the temperature T is 10^7 K which represents the temperature of the sporadic coronal condensation created at the flare. Those values are necessary only to evaluate the absorption of the radio burst as will be shown later.

The spectrum and polarization for the integrated emission from the preceding source alone (p – source in Figure 1) of the bipolar source will be treated in the following.

The self-absorption in the radio source is assumed to be small.

3. Gyro-Synchrotron Emission

The spectrum and polarization of the gyro-synchrotron emission from the model radiosource shown in the previous section are computed by using Equation (A-23) given in Appendix 4. Total flux $F(f)$ and polarization degree $P(f)$ are given by

$$F(f) = F_e(f) + F_0(f)$$
$$P(f) = [F_e(f) - F_0(f)]/F(f).$$

In deriving Equation (A-23), an effect of the ambient medium on the emissivity (Razin effect) is neglected and the refractive index is assumed to be unity, since the frequency range under consideration is above 10^3 MHz while the plasma frequency f_p is 285 MHz (for $N_0 = 10^9$ cm^{-3}) and the gyro-frequency f_H is comparable to or higher than f_p in the radio source (cf. Ramaty, 1969; Ramaty and Lingenfelter, 1967). It follows that the polarization ellipses for the extraordinary and ordinary modes are two circles with opposite senses of rotation, i.e. quasi-longitudinal approximation is valid.

4. Radio Bursts Occurring at the Center of the Solar Disk

The compution is simpler if the heliographic longitude ψ of the radio source is zero, so that the dependence of model on the spectrum and polarization is investigated mainly setting $\psi = 0$ as a first step.

If the energetic electrons are distributed spatially without any outer boundary in the corona in the present model of dipole field, the flux density increases monotonously with decreasing frequencies due to an increase of effective volume of radio source at lower frequencies. This is inconsistent with the observed spectra of microwave bursts. Accordingly an outer boundary is set and its effects on the spectrum and polarization are investigated. The intensity spectra are shown in Figure 3, and the polarization degrees are given in Table I. The energy distribution of non-thermal electrons is assumed as given in Appendix 2,

$$N(\varepsilon)\,\mathrm{d}\varepsilon = G\varepsilon^{-\gamma}\,\mathrm{d}\varepsilon,$$

and their integrated number density above 50 keV is indicated by N. The ordinate of Figure 3 is scaled by the flux density divided by N. In this figure, A and B correspond respectively to the models with the outer boundaries shown by curves A and B in Figure 2. The outer boundary for Model C is given by curves C and A in Figure 2, i.e., the energetic electrons are trapped only in a region below the curves C and A. The curve C shows a line of force, which passes a point $r=10^5$ km and $\lambda=60°$ (cf. Figure 2). The model C seems most realistic in order to satisfy the assumption that the energetic electrons are trapped in a part of the bipolar magnetic field. However,

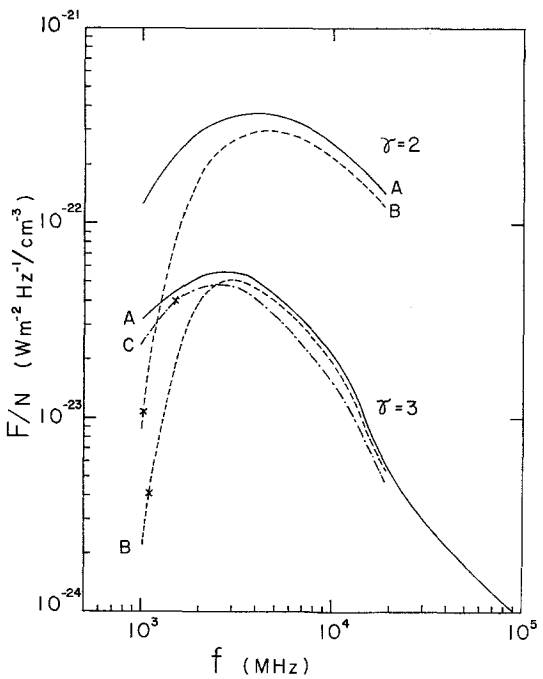

Fig. 3. Theoretical spectra of flux density for the radio bursts occurring at the center of the solar disk ($\psi=0$). A, B and C represent the model of outer boundary of radio source (cf. Figure 2). Crosses on the curves indicate a frequency at which the sense of circular polarization reverses. Polarization degree is given in Table I. Ordinate: Flux density F is divided by N which is an integrated number density of non-thermal electrons above 50 keV.

TABLE I

Circular polarization-degree (%)[a] of model burst at disk center ($\psi = 0$)

Model	γ	Frequency (GHz)					
		1.0	2.0	3.75	9.4	18.8	>100
A	3	3.4	19	36	61	33	0
B	3	− 4.3	15	34	62	35	0
C	3	−22	11	22	41	26	0
A	2	18	29	34	31	19	0
B	2	− 1.0	28	36	36	21	0

[a] Negative sign represents the sense of ordinary waves.

we can see from Figure 3 no essential difference between the spectra for Models C and A at least for the present case of $\psi = 0$, except for the polarization degree at 1000 MHz as shown in Table I. Therefore, the following treatment is made, for simplicity, only for Models A and B.

The spectrum and polarization at low frequencies depend strongly on the model of the outer boundary as shown in Figure 3 and Table I. The dependence decreases with increasing frequencies. At high frequencies at which only extremely relativistic electrons contribute to the emission, the spectrum tends to a model-independent spectral shape as $F \sim f^{(1-\gamma)/2}$ and the circular polarization degree tends to zero. Therefore, a few peculiar microwave bursts which showed increasing flux density with increasing frequencies even on millimeter wavelengths (Croom, 1969; Edelson, 1959) may infer that the exponent γ of the electron energy-distribution was near zero at least up to about 5 MeV in these special events. An alternative explanation would be that the radio source was optically thick for the self-absorption (Ramaty, 1969; Holt and Ramaty, 1969); γ may be $2 \sim 3$, but a high energy cutoff, if any, must be above 5 MeV. The optically thick case is, however, out of the scope of the present paper.

In almost all cases (e.g., Shiomi, 1969), the observed spectra of microwave impulsive bursts are similar to those shown in Figure 3, except that the frequency f_m at which the flux density of the burst shows a maximum is generally higher, say, by a factor 2 or 3. The most important parameters which determines f_m is the strongest magnetic field in the radio source: It is 1100 G in the present model (Figure 2). This value may be higher by a factor up to about 1.5 if the sunspot magnetic field is stronger (2500 G at the photosphere in the present model). Another most probable cause for the microwave bursts to show higher f_m is that the height of lower boundary of the radio source may be about 5×10^3 km or less (10^4 km in the present model as mentioned in Section 2) giving higher magnetic field by a factor of 1.4 or more as the strongest field in the radio source. Accordingly, the discrepancy between the theoretical f_m and observed f_m seems not serious.

The polarization degree shown in Table I seems consistent with the observed one.

The microwave impulsive bursts frequently show a reversal of sense of circular polarization at a frequency below f_m, and the sense of circular polarization is that of extraordinary waves at the higher frequencies and that of ordinary waves at the lower frequencies. In the present Modes B and C, the sense is for ordinary mode at 1000 MHz. This is attributed to the stronger absorption of extraordinary waves than the ordinary waves due to the thermal gyro-absorption (Figures A-6 and A-7 in Appendix). The optical thickness τ depends strongly on the temperature T of the thermal electrons: $\tau \sim T^{n-1}$ as given by Equation (A-18) in Appendix 3. At 1000 MHz where the effect of the absorption is strongest, therefore, the polarization degree and also intensity depend strongly on the temperature. If, for example, $T=3\times10^6$ K instead of 10^7 K adopted in the present model, the polarization degree at 1000 MHz for Model B ($\gamma=3$) reduces to -33% instead of -4.3% (see, Table I), and the flux density increases about one order compared with the value shown in Figure 3. Accordingly, some discrepancy between the theoretical polarization degree and observed one especially at 1000 MHz seems not serious.

It may be remarked that the above theoretical results correspond to a preceding half of whole radio source as mentioned in Section 2. Therefore, if the burst is observed without resolving the p and f sources (cf. Figure 1), the spectrum of the total emission from the whole radio source is a summation of emission from two sources with opposite senses of circular polarization taking into account a weight due to a difference of magnetic moments of the two dipoles. The polarization degree and the frequency at which the sense of circular polarization reverses depend on the unbalance of the two dipoles in this case. Interferometric observations of the microwave impulsive bursts with a fan beam of 1′ at Toyokawa have shown, however, that in some cases the sense reversal with frequency is seen on each radio source of bipolar structure (private communication, by courtesy of Mr. S. Enome, The Research Institute of Atmospherics, Nagoya University). Therefore, the sense reversal with frequency seems intrinsic in some cases, although the unbalance of the two dipoles may cause an apparent reversal (Takakura, 1967) and also the reversal may occur during the propagation (Cohen, 1961).

The contribution of each layer of radio source to the total emission is shown in Figure 4 for Model A and $\gamma=3$. Abscissa indicates the magnetic field strength of the layer. It is also scaled by the gyro-frequency f_H and by the height h of the layer at $\lambda=90°$. Ordinate shows the proportion of the integrated emission from the layers above a given equi-strength layer of the magnetic field, where $m=f/f_H$ and m_2 corresponds to the lowest value of f_H in the radio source; m_2 is 6 for 1 GHz, 12 for 2 GHz, 22.5 for 3.75 GHz and 56.5 for 9.4 GHz. From this diagram, we can deduce the effective range of m and effective height at each frequencies. As shown in this figure, the effective height of the radio source, e.g. the height to give the proportion of 0.5, decreases with increasing frequency up to about 9.4 GHz, and then increases at the higher frequencies tending to a curve shown by the chain curve ($f>100$ GHz). This inversion of the effective height is due to the slope of emissivity function shown in Figures A-2 and A-3 in the Appendix. The slope of the emissivity becomes less

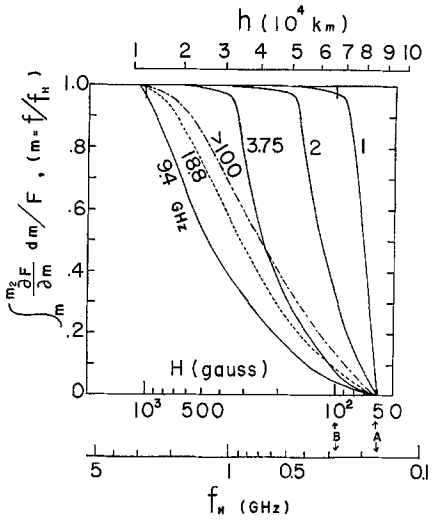

Fig. 4. The proportion of the integrated emissions from the radio source above a given equi-field-strength layer is plotted against the magnetic field strength of the layer: $\psi = 0$ and $\gamma = 3$. The abscissa is scaled also by the gyro-frequency f_H and the height h of the layer at $\lambda = 90°$ (cf. Figure 2). In the ordinate, m indicates f/f_H and an integration limit m_2 is for the outer boundary of the radio source; Model A in the present case. A and B on the abscissa show the outer boundaries for Models A and B, respectively. Numbers on the curves show the frequency of emission in GHz.

steep at the larger values of $m (m = f/f_H)$, which increases the weight of the layers with larger m (smaller magnetic field) at high frequencies.

As can be deduced from Figure 3, the number density of electrons N (integrated above 50 keV) which is required to emit a microwave burst with 100 flux unit (in 10^{-22} W m^{-2} Hz^{-1}) at f_m reduces to about 200 cm^{-3} for $\gamma = 3$ and about 30 cm^{-3} for $\gamma = 2$. These values are about the same order as estimated previously assuming a uniform magnetic field in the radio source (Takakura, 1969). The total number of energetic electrons above 50 keV in the whole radio source reduces to the order of 10^{32} for $\gamma = 3$ and 10^{31} for $\gamma = 2$, since the volume is of the order of 10^{30} cm^3 in the present model, although the effective volume at *each frequency* is about 0.1 or less of the whole radio source as can be deduced from Figure 4. These total numbers of energetic electrons are still two or three order smaller than the value estimated from hard X-ray bursts (Takakura, 1969).

Holt and Ramaty (1969) have attempted to explain this discrepancy taking the self-absorption into account and assuming that the X-rays and microwaves are produced by the common electrons in the same source. In their model, however, the suppression of radio flux at high frequencies, at which the radio source is required to be optically thin to give a negative spectral slope, is mainly attributed to either (i) the high energy cutoff (750 keV) or (ii) extremely anisotropic distribution of pitch angle of electrons. In the case (i), continuous acceleration of electrons is necessary during the decay phase of the event as they described, since the collision decay of electrons is faster than the decay time of the event. Also, very efficient acceleration

mechanism is required. Furthermore, higher energy electrons (>750 keV) should emit stronger radio waves at the high frequencies during their acceleration up to above 3 MeV and until they escape into smaller magnetic field, since such electrons were detected in the interplanetary space at this event. Although the duration of the corresponding radio impulse may be of the order of second, the strong peak may be recorded with usual radiometers with time resolution of 0.5 sec or so. In the case (ii), the extremely anisotropic distribution ($g(\varphi)=\sin^{45}\varphi$) gives strong directivity so that the radio emission is strongly suppressed in the *unfavourable* direction of observation as they tentatively chose ($\theta=45°$). It means that the ratio of X-ray flux to radio flux depends strongly on the direction of observation θ, in other words, the ratio may scatter from event to event in a wide range of several orders of magnitude. This is inconsistent with the observed rather good correlation between the fluxes of X-ray bursts and radio bursts. The above is a reason why we have treated optically thin source in the present paper. Incidentally we should point out that even though the emitting sources of X-rays and radio waves are distinct like the model by Takakura and Kai (1966), temporal correlation between the peaks of radio bursts and X-rays may be high if the acceleration of electrons is common, since the sub-peaks in the time history may correspond to additional accelerations. It also may be noted that *e*-folding times of radio bursts and X-ray bursts are generally different. However, non-uniform model which is optically thick at lower frequencies would be worth studying. In this case, it is required for the non-uniform model common to the micro-waves and X-rays, if any, that a product of effective volume emissivity η and effective volume V must be the same order as the present model at 9.4 GHz under much higher number density N by several orders of magnitude, since the source is required to be optically thin generally at 9.4 GHz. It infers that the effective magnetic field is very low to have low emissivity at high frequencies and/or the effective volume is very small compared with the present model. It may be worth noting that if the source is optically thick at low frequencies, the peak in time history is required to be broader due to the saturation at low frequencies compared with high frequencies.

5. Center to Limb Variation

The center to limb variations in the intensity, polarization and effective height are investigated in a comparison among those for $\psi=45°$, $90°$ and for $\psi=0$ given in the previous section. Intensity spectra for Models A and B ($\gamma=3$) are shown in Figures 5 and 6 respectively, and the intensity ratios are tabulated in Table II. As seen from these figures and Table II the center to limb variation in intensity is rather small and it is of the same order as derived statistically from the observations (Kakinuma *et al.* 1969; Scalise, 1970). A tendency can be seen in Figures 5 and 6 that the broad peak of the spectra shifts towards higher frequencies near the limb. It follows that a ratio of flux densities at 9.4 GHz and 3.75 GHz, $F(9.4)/F(3.75)$, increases near the limb. This is consistent with the statistical result derived by Scalise (1970). The increase in flux density at $\psi=90°$ on the theoretical spectra at high frequencies is attributed to

an increase in an effective volume with θ near 90° around which emissivity function is maximum (see Figures A-2 to A-5 in Appendix), while the decrease in flux density at low frequencies at $\psi = 90°$ is due to an increase in an optical thickness of gyro-absorption layers: θ is an angle between the magnetic field and the ray direction. Such a difference with frequency is due to a difference of effective range of m with frequency (cf. Figures 4 and 7). At low frequencies, the range of m is small at which the effect of absorption is strong.

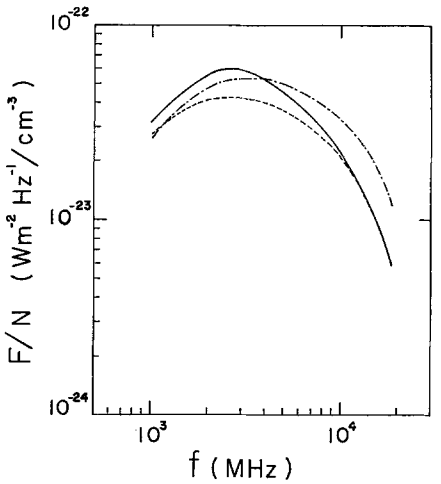

Fig. 5. Center to limb variation of the theoretical spectra of flux density: $\gamma = 3$ and Model A. Solid curve is for the bursts occurring at the center of the solar disk ($\psi = 0°$), dashed curve is for $\psi = 45°$ and chain curve is for the limb burst ($\psi = 90°$). Ordinate scale is same as Figure 3. Polarization degree is given in Table III.

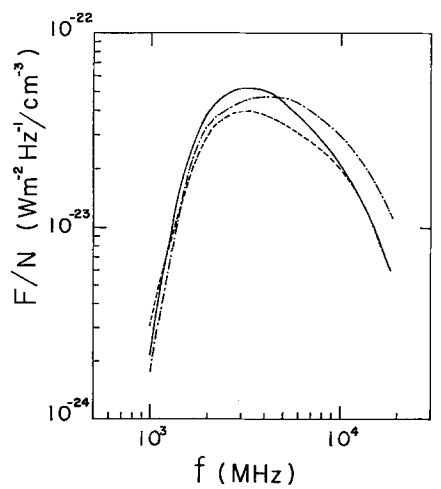

Fig. 6. Center to limb variation of the theoretical spectra: $\gamma = 3$ and Model B. The others are the same as shown in the caption to Figure 5.

The center to limb variation in the degree of circular polarization is tabulated in Table III. The decrease in polarization degree near the limb is remarkable at high frequencies, and it is consistent with the statistical result (Kakinuma *et al.* 1969; Scalise, 1970). It is attributed to an increase in the effective volume with θ near 90° at which the polarization degree tends to zero. On the other hand, the polarization degree at 1000 MHz increases at the limb showing the sense of extraordinary waves. This is attributed to that increase in the optical thickness of the gyro-absorption layers which results in a shift of the effective range of θ towards smaller angles at which a ratio of extraordinary and ordinary components is large (cf. Figures A-2 and A-3). The effective range of θ depends strongly on the temperature of the thermal electrons

TABLE II

Center to limb variation in intensity ratio ($F(\psi)/F(\psi=0)$)

Model ($\gamma=3$)	ψ	Frequency (GHz)				
		1.0	2.0	3.75	9.4	18.8
A	45°	0.93	0.77	0.75	0.88	0.98
	90°	0.91	0.91	1.00	1.34	2.00
B	45°	1.43	0.82	0.74	0.91	1.00
	90°	0.80	0.88	0.97	1.30	2.14
Statistical	$\frac{F(30°\sim 60°)}{F(0°\sim 30°)}$	0.74	0.80	0.89	0.83	–
Kakinuma *et al.*	$\frac{F(60°\sim 90°)}{F(0°\sim 30°)}$	0.60	0.66	0.71	0.66	–
Scalise	$\frac{F(60°\sim 90°)}{F(0°\sim 15°)}$	1.5	1.0	0.67	1.5	–

TABLE III

Center to limb variation in circular polarization-degree[a] (%)

Model ($\gamma=3$)	ψ	Frequency (GHz)					
		1.0	2.0	3.75	9.4	18.8	>100
A	0°	3.4	19	36	61	33	0
	45°	37	39	54	60	30	0
	90°	17	22	22	12	15	0
B	0°	− 4.3	15	34	62	35	0
	45°	20	40	57	61	32	0
	90°	19	20	23	13	16	0

[a] Negative sign represents the sense of ordinary waves.

as remaked in the previous section, so that the degree of polarization at 1000 MHz is strongly model dependent.

The center to limb variations of intensity and polarization are thus consistent with observed results. For the more quantitative discussion, the present model seems too simple and also the observational results have some ambiguities. It may be noted again that the above theoretical results correspond to the preceding half of the bipolar burst-source occurring in the west hemisphere of the solar disk (or following half in the east hemisphere). Following half and preceding half of a burst-source give the opposite senses of circular polarization at the source. Therefore, the polarization degree of integrated emission from the whole source is determined by the unbalance of the bipolar radio source when the radio source is in the central zone of the solar disk. However, when the radio source is far from the disk center, the polarization sense of the emission from one of these may reverse during the propagation in a quasi-transverse region leading to the same sense at the observer on an analogy of the limiting polarization of S-components (Takakura, 1961).

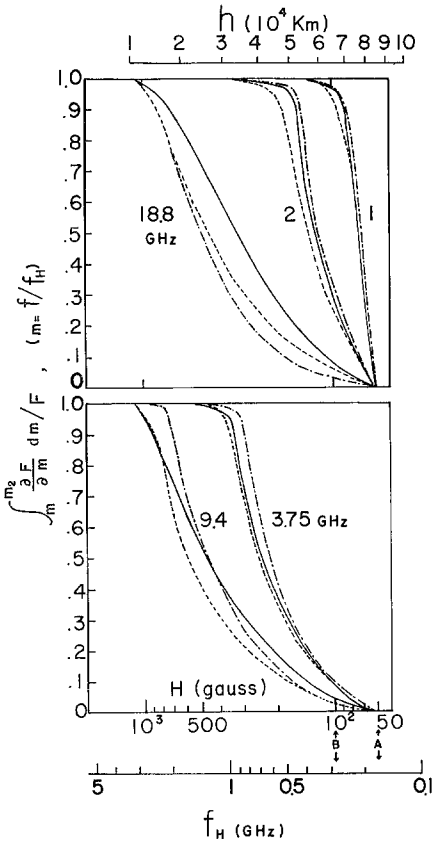

Fig. 7. Center to limb variation of the effective layer of the radio source: $\gamma = 3$ and Model A. See the caption to Figure 4. Solid curve, $\psi = 0$; Dashed curve, $\psi = 45$; Chain curve, $\psi = 90°$.

The center-limb variation in an effective height is shown in Figure 7. The variation is not great. There is a tendency that at very high frequencies the effective height decreases with the longitude ψ, while at lower frequencies the effective height is lowest around $\psi = 45°$.

6. Conclusion

A magnetic field caused by a vertical magnetic dipole situated 0.05 solar radii below the photosphere is adopted as the magnetic field in the radio source emitting a microwave impulsive burst. This model can reasonably account for the spectrum and polarization and also their statistical center-limb variations of observed microwave impulsive bursts.

The frequency f_m at which the flux density shows a maximum is mainly determined by the strongest magnetic field-strength in the radio source. The observed decrease in flux density towards lower frequency is mostly attributed to the outer boundary of the radio source, in other words, the lowest magnetic field in the radio source determines the low frequency cut-off. The effect of nonuniform magnetic field decreases with frequencies and at very high frequencies, the spectral index tends to $(1-\gamma)/2$ even if the magnetic field is not uniform in the radio source.

The influence of the ambient plasma on the emission (Razin effect) is not effective in the present model. However, if the density of the ambient medium is higher and/or the magnetic field is lower than the present model, the Razin effect cannot be ignored, which results in a reduction of the flux at low frequencies (Ramaty, 1969) especially near 1000 MHz.

The center to limb variation in intensity is not great due to the distribution of θ in the radio source, though the emissivity depends strongly on θ especially at small values of θ. Near the limb, the flux density increases at high frequencies due to an increase in effective volume with θ near 90°, while at the lower frequencies the flux density decreases due to an increase in the optical thickness of gyro-absorption layers. It follows that a broad peak of the spectrum shifts slightly towards higher frequencies near the limb.

The sense of circular polarization at high frequencies is that of extraordinary waves which is intrinsic for the gyro-synchrotron emission, while at low frequencies the sense may reverse to that of ordinary waves due to the selective absorption of extraordinary component at the resonance layers of thermal gyro-absorption. The sense and degree of circular polarization are strongly model dependent at low frequencies. The circular polarization-degree tends to zero at high frequencies ($f > 10^5$ MHz) at which only extremely relativistic electrons contribute to the emission. The degree of polarization decreases near the limb at high frequencies due to an increase in an effective volume with θ near 90° at which the polarization degree tends to zero.

An effective height of the radio source depends on the frequency due to both a decrease in the gyro-frequency f_H with height and the dependence of emissivity function on f/f_H. In the present model, the effective height is about 8×10^4 km at 1 GHz, decreases with frequency and 3×10^4 km at 9.4 GHz and then increases with frequency

up to about 4.5×10^4 km at higher frequencies. The center-limb variation of the effective height is not great. At very high frequencies, the effective height decreases with the heliographic longitude ψ by a factor of about 0.8 at the limb.

In order to emit a microwave burst with 100 unit (in 10^{-22} W m^{-2} Hz^{-1}) at 3 GHz, the number density of non-thermal electrons integrated above 50 keV reduces to about 200 cm^{-3} for $\gamma=3$ and 30 cm^{-3} for $\gamma=2$. The total volume of the radio source in which those electrons are trapped in the present model is of the order of 10^{30} cm^3, although an effective volume *at each frequency* is $10 \sim 3\%$ of the whole volume.

Appendix 1. Magnetic Configuration in the Radio Source

A dipole magnetic field is given by the following equations. The coordinate system is shown in Figure A-1.

The lines of force are given by

$$r = C \cos^2 \lambda \tag{A-1}$$

changing the constant C.

A surface with equal magnetic field-strength H (or gyro-frequency f_H) is given by

$$r = d\left(\frac{H_0}{2H}\right)^{1/3} (1 + 3 \sin^2 \lambda)^{1/6}, \tag{A-2}$$

$$= d\left(\frac{f_H(0)}{2f_H}\right)^{1/3} (1 + 3 \sin^2 \lambda)^{1/6}, \tag{A-2'}$$

where d is the depth of the vertical dipole below the photosphere, $d=3.5 \times 10^4$ km

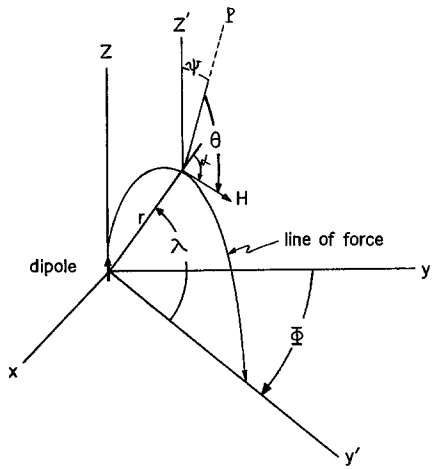

Fig. A-1. Coordinate for a dipole magnetic field. *A y–z* plane is the ecliptic plane on which a distant observer *P* is located.

in the present model, H_0 is the magnetic field strength at the photosphere on the axis of the dipole and $f_H(0)$ is the gyro-frequency for H_0.

An angle θ between the direction of observer and a line of force is given as a function of ψ, Φ and λ (cf. Figure A-1),

$$\cos\theta = \sin\psi\cos(\lambda-\alpha)\cos\Phi + \cos\psi\sin(\lambda-\alpha), \tag{A-3}$$

and

$$\tan\alpha = \tfrac{1}{2}\cot\lambda. \tag{A-4}$$

A volume element in which θ is θ to $\theta+\mathrm{d}\theta$ and the magnetic field-strength is H to $H+\mathrm{d}H$ is given by

$$\mathrm{d}V = r\cos\lambda\sqrt{r^2+(\partial r/\partial\lambda)^2}\,\mathrm{d}\Phi\,\mathrm{d}\lambda\,\mathrm{d}r, \tag{A-5}$$

by using Equations (A-2) to (A-4). Equation (A-5) reduces to

$$\mathrm{d}V = \frac{\mathrm{d}^3}{6}\frac{f_H(0)}{f}\sin\theta\cos\lambda\left[(1+3\sin^2\lambda)\left\{1+\left(\frac{\sin\lambda\cos\lambda}{1+3\sin^2\lambda}\right)^2\right\}\right]^{1/2} \times\left[\{\sin\psi\cos(\lambda-\alpha)\}^2-\{\cos\theta-\cos\psi\sin(\lambda-\alpha)\}^2\right]^{-1/2}\mathrm{d}\theta\,\mathrm{d}\lambda\,\mathrm{d}m \tag{A-6}$$

where $m\equiv f/f_H=(H_0/H)(f/f_H(0))$, f is the frequency of emission under consideration and f_H is the gyro-frequency for H.

Appendix 2. Gyro-Synchrotron Emission

The general formulae of the volume emissivity of gyro-synchrotron emission from an ensemble of electrons were given by Kawabata (1964) and some computations were made by Takakura *et al.* (1968). Those, however, were incorrect by a factor

$$(nf_H/f)(1+p^2)^{-1/2} \quad \text{or} \quad \{1-p(1+p^2)^{-1/2}\cos\theta\cos\varphi\}$$

in the integrand (Takakura and Uchida, 1968 and 1969).

The corrected volume emissivity of intensity η_{R+L} is given, for $\theta\neq 90°$,

$$\eta_{R+L}(f,\theta) = \frac{(2\pi e)^2 f}{c\cos\theta}\sum_n\int_{p_1}^{p_2}(a^2+b^2)\frac{p}{\sqrt{1+p^2}}N(p,\varphi)\,\mathrm{d}p, \tag{A-7}$$

where

$$a = p\sin\varphi\,J_n'(x),$$

$$b = \frac{\sqrt{1+p^2}\cos\theta - p\cos\varphi}{\sin\theta}J_n(x),$$

$$x = fp\sin\varphi\sin\theta/f_H,$$

p_1 and p_2 are positive roots of the equation, which gives the frequency of emission,

$$f = nf_H(\sqrt{1+p^2} - p\cos\varphi\cos\theta)^{-1} \tag{A-8}$$

setting $\cos\varphi = \pm 1$, and in the integrand

$$\cos\varphi = \frac{\sqrt{1+p^2} - (nf_H/f)}{p\cos\theta}. \tag{A-9}$$

The summation over n is to be carried out for $n > f\sin\theta/f_H$.

The circularly polarized component of the volume emissivity is given by, for $\theta \neq 90°$,

$$\eta_{R-L}(f,\theta) = \frac{(2\pi e)^2 f}{c\cos\theta} \sum_n \int_{p_1}^{p_2} 2a\cdot b \frac{p}{\sqrt{1+p^2}} N(p,\varphi)\,dp. \tag{A-10}$$

If the refractive index is near unity in the plasma like the present case, the polarization ellipses for the two characteristic modes, extraordinary and ordinary, are approximately two circles with opposite senses of rotation (quasi-longitudinal approxi-

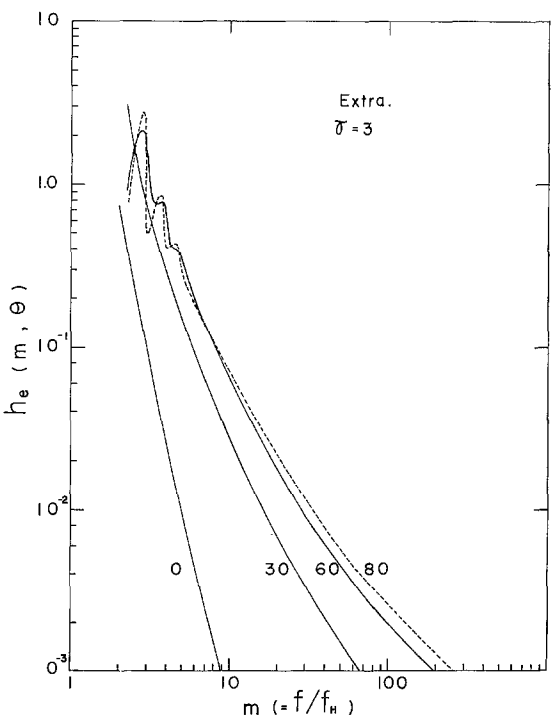

Fig. A-2. Volume emissivity η_e for the extraordinary mode is plotted against f/f_H: $\gamma = 3$. The ordinate is scaled by $c\eta_e/G\pi\, e^2 f_H \equiv h_e(m,\theta)$. θ is indicated on the curves. At high frequencies above $m = 10^2$, an extremely relativistic approximation is used leading to $h_e(m,\theta) \sim m^{-1}(\sin\theta)^2$.

mation). Then we have the volume emissivities η_e and η_0 for the each mode, for $\theta \neq 90°$,

$$\eta_{e,0}(f, \theta) = \tfrac{1}{2}(\eta_{R+L} \pm \eta_{R-L})$$
$$= \frac{(2\pi e)^2 f_H}{c} \frac{f}{2f_H \cos\theta} \sum_n \int_{p_1}^{p_2} (a \pm b)^2 \frac{p}{\sqrt{1+p^2}} N(p, \varphi)\, \mathrm{d}p, \tag{A-11}$$

where the upper and lower signs correspond to the extraordinary wave and ordinary wave, respectively.

If the distribution of pitch angle φ of electrons is isotropic and the energy distribution is $N(\varepsilon)\, \mathrm{d}\varepsilon = G\varepsilon^{-\gamma}\, \mathrm{d}\varepsilon$,

$$4\pi p^2 N(p, \varphi)\, \mathrm{d}p = N(\varepsilon)\, \mathrm{d}\varepsilon$$

so that we have

$$N(p, \varphi) = \frac{G}{4\pi} p^{-1}(1+p^2)^{-1/2}(\sqrt{1+p^2} - 1)^{-\gamma}, \tag{A-12}$$

where $p = mv/m_0 c$ and $\varepsilon = K/m_0 c^2$; $(1+\varepsilon)^2 = 1 + p^2$. In an assumption that $\gamma = 3$ or 2

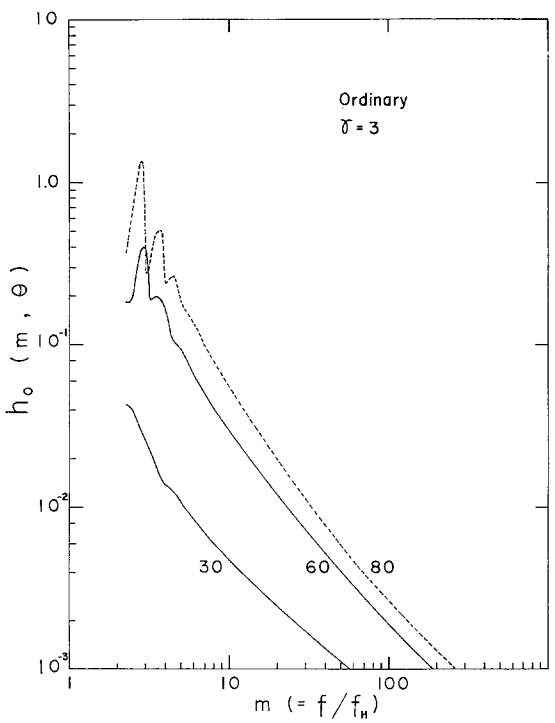

Fig. A-3. Volume emissivity η_0 for the ordinary mode: $\gamma = 3$. The ordinate is scaled by $c\eta_0/G\pi e^2 f_H \equiv h_0(m, \theta)$. The others are the same as shown in the caption to Figure A-2. $h_0(m, \theta) = 0$ at $\theta = 0$ for the ordinary mode.

in a range $p \geqslant 0.3$ ($K \geqslant 23$ keV) and $N(p, \varphi)=0$ for $p<0.3$, volume emissivities η_e and η_0 are potted against m ($m=f/f_H$) in Figures A-2 to A-5. It may be noted that at $\theta=0$, $\eta_0=0$ but $\eta_e \neq 0$. At very high frequencies, $m \gtrsim 100$, an extremely relativistic approximation is used for the computation of the emissivity (cf. Takakura, 1967). In this case, η_e and η_0 are nearly proportional to $f^{(1-\gamma)/2}(\sin\theta)^{(1+\gamma)/2}$ as is well known, and $\eta_e \approx \eta_0$ except for very small values of θ.

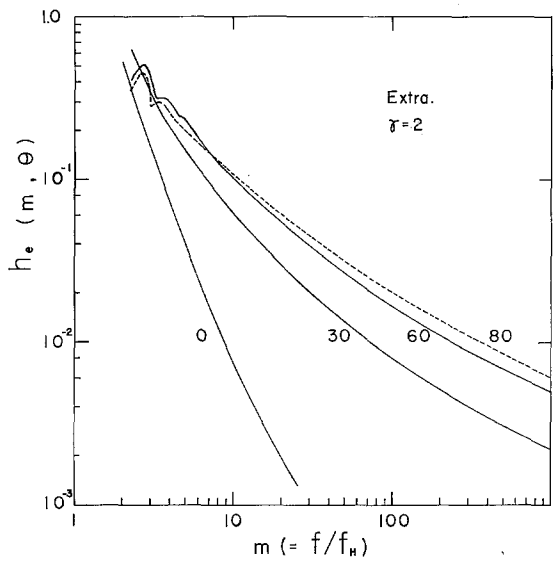

Fig. A-4. Volume emissivity for the extraordinary mode: $\gamma=2$. Refer to the caption to Figure A-2. At high frequencies above $m=10^2$, $h_e(m, \theta) \sim m^{-1/2}(\sin\theta)^{3/2}$.

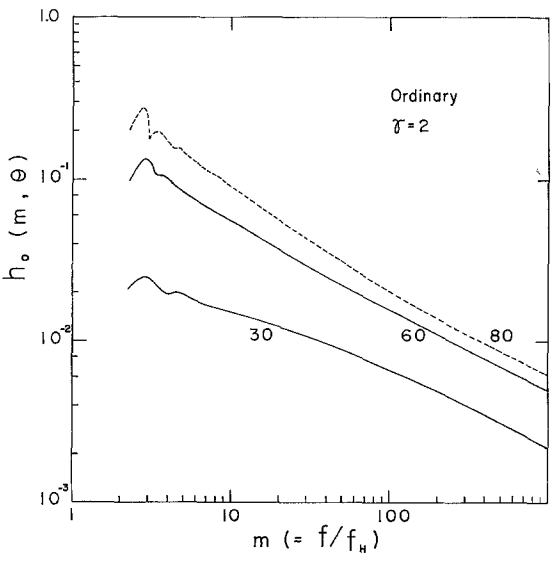

Fig. A-5. Volume emissivity for the ordinary mode: $\gamma=2$. Refer to the caption to Figure A-3.

Appendix 3. Thermal Gyro-Absorption

The absorption coefficient of the thermal gyro-absorption has been given by several workers. Here, the formulae reduced by Kai (1965) from the general formulae by Kawabata (1964) are used since these seem convenient for the computation. The absorption coefficients at the nth harmonics of the gyro-frequency f_H are given for the extraordinary wave κ_e and for the ordinary wave κ_0,

$$\kappa_e(n,\theta) \simeq N_0 \frac{(2\pi e)^2 n^{2n-1}}{\pi^{3/2} m_0 c f_H 2^{2n} n!} \xi^{n-(3/2)} (\sin\theta)^{2n-2} \times \frac{(c_1 + c_2 \cos\theta)^2}{\cos\theta} \exp\left\{ - \frac{\left(1 - \frac{n f_H}{f}\right)^2}{\xi \cos^2\theta} \right\} \tag{A-13}$$

$$\kappa_0(n,\theta) \simeq N_0 \frac{(2\pi e)^2 n^{2n-1}}{\pi^{3/2} m_0 c f_H 2^{2n} n!} \xi^{n-(3/2)} (\sin\theta)^{2n-2} \times \frac{(c_2 - c_1 \cos\theta)^2}{\cos\theta} \exp\left\{ - \frac{\left(1 - \frac{n f_H}{f}\right)^2}{\xi \cos^2\theta} \right\} \tag{A-14}$$

where N_0 is the number density of thermal electrons, $\xi = 2kT/m_0c^2$,

$$c_1 = \frac{\frac{y_T^2}{2(1-x)} + \left\{ \frac{y_T^4}{4(1-x)^2} + y_L^2 \right\}^{1/2}}{\left[2y_L^2 + \frac{y_T^4}{2(1-x)^2} + \frac{y_T^2}{1-x} \left\{ \frac{y_T^4}{4(1-x)^2} + y_L^2 \right\}^{1/2} \right]^{1/2}},$$

$$c_2 = \frac{y_L}{\left[2y_L^2 + \frac{y_T^4}{2(1-x)^2} + \frac{y_T^2}{1-x} \left\{ \frac{y_T^4}{4(1-x)^2} + y_L^2 \right\}^{1/2} \right]^{1/2}},$$

$$x = (f_p/f)^2, \qquad y_L = y\cos\theta, \qquad y_T = y\sin\theta \quad \text{and} \quad y = f_H/f\,.$$

Setting $N_0 = 10^9\ \mathrm{cm}^{-3}$ and $T = 10^7$ K which may represent the temperature of the sporadic coronal condensation during the flare, we have the absorption coefficients at the line center ($f_H = f/n$) as shown in Figures A-6 and A-7.

The optical thickness along the line of sight is given by

$$\begin{aligned} &\tau_{e,0}(n,\theta) = \kappa_{e,0}(n,\theta)\, \Delta r/\cos(\theta - \alpha), \\ &\cos(\theta - \alpha) = \sin\psi \cos\lambda \cos\Phi + \cos\psi \sin\lambda, \end{aligned} \tag{A-15}$$

where Δr is the effective thickness along the radius vector which is nearly parallel to the gradient of the magnetic field-strength. This thickness corresponds to an effective width of the absorption line around $f_H = f/n$. The profile of the absorption line is

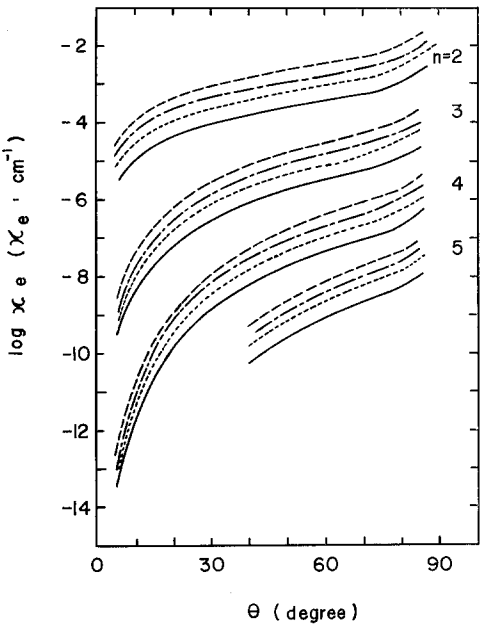

Fig. A-6. Thermal gyro-absorption coefficient for the extraordinary waves κ_e at the line center of the nth harmonic of gyro-frequency is plotted against θ: $T=10^7$ K and $N_0=10^9$ cm^{-3}. Harmonic number n is indicated on the curves. Solid curve, 9.4 GHz; Dotted curve, 3.75 GHz; Chain curve, 2 GHz; Dashed curve, 1 GHz.

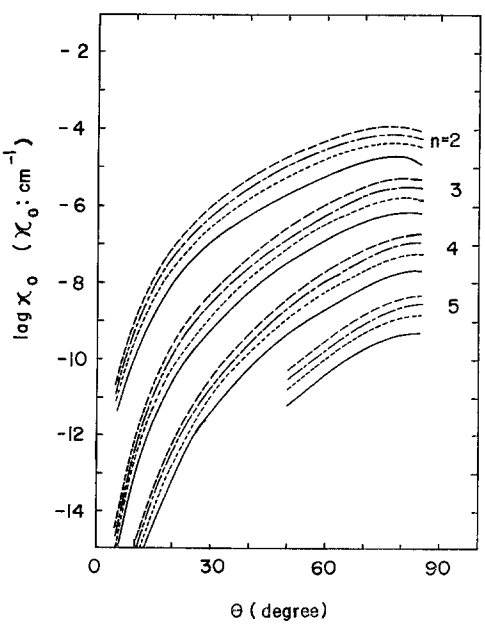

Fig. A-7. Thermal gyro-absorption coefficient for the ordinary waves. The others are the same as shown in the caption to Figure A-6.

given by the last factor in Equations (A-13) and (A-14), i.e.

$$\exp\left\{-\frac{\left(1-\frac{nf_H}{f}\right)^2}{\xi\cos^2\theta}\right\},$$

where f is given and f_H is a variable. This factor is unity at the line center at $f_H=f/n$ and $1/e$ at

$$f_H=\frac{f}{n}(1\pm\delta).$$

This small deviation δ from the line center corresponds to $\mp\Delta r/2$ in the radius vector. The δ and Δr are equated as

$$\frac{\partial f_H}{\partial r}\frac{\Delta r}{2}=-\frac{f}{n}\delta. \tag{A-16}$$

From this and Equation (A-2′), we have

$$\begin{aligned}\Delta r&=\frac{2}{3}\frac{f}{nf_H}|\cos\theta|\sqrt{\xi}\,r\\&\approx\tfrac{2}{3}|\cos\theta|\sqrt{\xi}\,r.\end{aligned} \tag{A-17}$$

Accordingly Equation (A-15) reduces to

$$\tau_{e,0}(n,\theta)=\frac{\frac{2}{3}|\cos\theta|\sqrt{\xi}\,\kappa_{e,0}(n,\theta)\,r}{\sin\psi\cos\lambda\cos\Phi+\cos\psi\sin\lambda}, \tag{A-18}$$

which is proportional to T^{n-1}.

Appendix 4. The Spectrum of Gyro-Synchrotron Emission

The spectrum and polarization of the emission from the radio source can be computed from Equations (A-6), (A-11), (A-12) and (A-18) for two modes of wave. The flux density $\mathrm{d}F$ at the distance R of the earth due to the emission from a volume element $\mathrm{d}V$ given by Equation (A-6) is given by

$$\mathrm{d}F=\frac{\eta\,\mathrm{d}V}{R^2}\exp(-\tau). \tag{A-19}$$

The absorption factor $\exp(-\tau)$ is necessary only at smaller m ($m=f/f_H$) than 5 in the present model: The absorption is not negligible even at the 5th harmonic layer if $T=10^7$ K as adopted in the present model. For example, the emissions at a given frequency f from the layers with m between 2 and 3 ($f/2>f_H>f/3$) pass through the overlying absorption layers of the 3rd harmonic ($n=3$) and higher harmonics ($n>4$) of the gyro-frequency. In this case κ at the 3rd harmonic layer is about 2 order larger than that of the 4th harmonic layer (cf. Figures A-6, A-7) so that the absorption only

at $n=3$ is enough to be taken into account. In the same way, the emissions from the layers of $3<m<4$ suffer absorption at the 4th harmonic layer ($n=4$).

Now, the ordinate in Figures A-2 to A-5 is scaled by

$$\frac{c}{G\pi\, e^2 f_H}\eta_{e,0}(f,\theta) \equiv h_{e,0}(m,\theta). \tag{A-20}$$

By using this notation, we have from Equations (A-19) and (A-6)

$$dF_{e,0} = \frac{G\pi\, e^2 d^3 f_H(0)}{6cR^2}\frac{1}{m} h_{e,0}(m,\theta)\, k(\psi,\theta,\lambda)\exp(-\tau_{e,0})\,\mathrm{d}\theta\,\mathrm{d}\lambda\,\mathrm{d}m, \tag{A-21}$$

where

$$k(\psi,\theta,\lambda) = \sin\theta\cos\lambda\left[(1+3\sin^2\lambda)\left\{1+\left(\frac{\sin\lambda\cos\lambda}{1+3\sin^2\lambda}\right)^2\right\}\right]^{1/2} \times\left[\{\sin\psi\cos(\lambda-\alpha)\}^2-\{\cos\theta-\cos\psi\sin(\lambda-\alpha)\}^2\right]^{-1/2} \tag{A-22}$$

and $\tan\alpha=\frac{1}{2}\cot\lambda$. The flux density due to the whole radio source reduces to

$$F_{e,0}(f) = \frac{G\pi\, e^2 d^3 f_H(0)}{6cR^2}\left\{\sum_{n=2}^{4}\int_n^{n+1}\frac{1}{m}H_{e,0}(\psi, f/m)\,\mathrm{d}m + \int_5^{m_2(f)}\frac{1}{m}H_{e,0}(\psi, f/m)\,\mathrm{d}m\right\} \tag{A-23}$$

and

$$H_{e,0}(\psi, f/m) = \int_{\theta_1(\psi,f/m)}^{\theta_2(\psi,f/m)} h_{e,0}(m,\theta)\,K(\psi,\theta)\exp\{-\tau_{e,0}(n+1,\theta)\}\,\mathrm{d}\theta \qquad \text{for} \quad m\leqslant 5$$

$$= \int_{\theta_1}^{\theta_2} h_{e,0}(m,\theta)\,K(\psi,\theta)\,\mathrm{d}\theta \qquad \text{for} \quad m>5,$$

$$K(\psi,\theta) = \int_{\lambda_1(\psi,\theta)}^{\lambda_2(\psi,\theta)} k(\psi,\theta,\lambda)\,\mathrm{d}\lambda,$$

where the integration limits λ_1, λ_2, θ_1, θ_2 and m_2 are determined by the boundaries of the radio source. The optical thickness $\tau_{e,0}$ is not only the function of θ and ψ, but also depends on r, λ and Φ as shown in Equation (A-18), and these vary along a curve for a fixed θ on a given absorption layer. However, the variation in $r/(\sin\psi\cos\lambda\cos\Phi+\cos\psi\sin\lambda)$ on a given harmonic layer is not so large in a range $0.1<\tau<3$ (otherwise $e^{-\tau}$ may be set to 1 or zero) so that this value was set, for simplicity, as a constant on each given harmonic layer in the present computation.

The θ at the absorption layer is not the same as that of the emitting layer, but the same value is used in the present computation, for simplicity, since the difference is generally not so large.

The first term in the bracket of Equation (A-23) gives the emission from the layers in which m is between 2 and 5, if any. The contribution from the layers with m less than 2 is negligible due to the strong thermal gyro-absorption of both wave modes at the 2nd harmonic layer ($n=2$) or at the fundamental layer ($n=1$).

The total flux is given by

$$F = F_e + F_0 ,$$

and the polarization degree is given by

$$P = (F_e - F_0)/F .$$

References

Chang, D. B. and Davis, L. Jr.: 1962, *Astrophys. J.* **136**, 567.
Cohen, M.: 1961, *Astrophys. J.* **133**, 978.
Croom, D. L. and Powell, R. J.: 1969, *Nature* **221**, 945.
Edelson, S.: 1959, private communication; an event at 17:05 UT on Dec. 1, 1959.
Holt, S. S. and Ramaty, R.: 1969, *Solar Phys.* **8**, 119.
Kai, K.: 1965, *Publ. Astron. Soc. Japan* **17**, 309.
Kakinuma, T., Yamashita, T., and Enome, S.: 1969, *Proc. Res. Inst. Atmospherics, Nagoya Univ.* **16**, 127.
Kawabata, K.: 1964, *Publ. Astron. Soc. Japan* **16**, 30.
Ramaty, R. and Lingenfelter, R. E.: 1967, *J. Geophys. Res.* **72**, 879.
Ramaty, R.: 1969, NASA Preprint X-611-69-23.
Scalise, E., Jr.: 1970, *Publ. Astron. Soc. Japan* (to be published).
Shiomi, Y.: 1969, *Solar Phys.* **6**, 276.
Takakura, T.: 1961, *Publ. Astron. Soc. Japan* **13**, 312.
Takakura, T.: 1967, *Solar Phys.* **1**, 304.
Takakura, T.: 1969, *Solar Phys.* **6**, 133.
Takakura, T., Uchida, Y., and Kai, K.: 1968, *Solar Phys.* **4**, 45.
Takakura, T. and Kai, K.: 1966, *Publ. Astron. Soc. Japan* **18**, 57.
Takakura, T. and Uchida, Y.: 1968, *Astrophys. Letters* **2**, 87.
Takakura, T. and Uchida, Y.: 1969, *Solar Phys.* **6**, Corrigenda (last page).